



UNIVERSITY OF LEEDS

This is a repository copy of *Atomic structure and phase assemblages in novel M-(N)-A-S-H materials*.

White Rose Research Online URL for this paper:
<https://eprints.whiterose.ac.uk/173947/>

Version: Accepted Version

Article:

Bedeaux, M, Gevaudan, JP, Lama, B et al. (1 more author) (2021) Atomic structure and phase assemblages in novel M-(N)-A-S-H materials. *Cement and Concrete Research*, 142. 106336. ISSN 0008-8846

<https://doi.org/10.1016/j.cemconres.2020.106336>

© 2020, Elsevier. This manuscript version is made available under the CC-BY-NC-ND 4.0 license <http://creativecommons.org/licenses/by-nc-nd/4.0/>.

Reuse

This article is distributed under the terms of the Creative Commons Attribution-NonCommercial-NoDerivs (CC BY-NC-ND) licence. This licence only allows you to download this work and share it with others as long as you credit the authors, but you can't change the article in any way or use it commercially. More information and the full terms of the licence here: <https://creativecommons.org/licenses/>

Takedown

If you consider content in White Rose Research Online to be in breach of UK law, please notify us by emailing eprints@whiterose.ac.uk including the URL of the record and the reason for the withdrawal request.



eprints@whiterose.ac.uk
<https://eprints.whiterose.ac.uk/>

Atomic Structure and Phase Assemblages in Novel M-(N)-A-S-H Materials

Matthew Bedeaux¹, Juan Pablo Gevaudan^{2†}, Bimala Lama³, Wil V. Srubar III^{4,5}

¹Department of Chemical and Biological Engineering, University of Colorado Boulder, United States of America (USA) ²School of Civil Engineering, University of Leeds, United Kingdom (UK) ³Department of Chemistry, University of Colorado Boulder, ⁴Department of Civil, Environmental, and Architectural Engineering, University of Colorado Boulder ⁵Materials Science and Engineering Program, University of Colorado Boulder;

†Corresponding Author: j.p.gevaudan@leeds.ac.uk

Abstract

This paper investigates the atomic structure and phase assemblages in new sodium-stabilized magnesium aluminosilicate hydrate (M-(N)-A-S-H) cementitious binders. Results indicate that in the absence of Ca^{2+} , Mg^{2+} promotes a binder atomic structure of Si-Al tetrahedral sheets and octahedral Mg sheets with hydrated Na^+ cations likely in the interlayer sites similar to trioctahedral micas (phyllosilicates). NMR studies verify the incorporation of Al in tetrahedral silicate sheets. XRD demonstrates the ability of these regions to nucleate and form zeolites (*i.e.*, sodalite) as well as the formation of Mg-Al layered double hydroxide (LDH) phases (*i.e.*, meixnerite), which is expected due to high concentrations of Mg and Al. TGA results indicate that M-(N)-A-S-H possesses chemically bound water and hydroxyl units similar to other Mg binders. These results evidence the critical role of Mg to form unique atomic structures and durability-related phases in low-calcium alkali-activated materials.

Keywords: alkali activated cements, layered double hydroxide phases, magnesium, nuclear magnetic resonance.

1. Introduction

Alkali-activated materials (AAMs) are promising alternatives to ordinary portland cement (OPC) due to potentially lower CO_2 emissions and improved durability in select applications. AAMs are produced by mixing alkaline solutions with silicon- (Si) and aluminum-rich (Al) industrial byproducts (*e.g.*, slag, fly ash). AAM production has been estimated to emit 50-80% less CO_2 compared to the production of OPC

which currently accounts for 6% of global CO₂ emissions [1]. Additionally, current research has demonstrated that AAMs exhibit improved durability (*e.g.*, acid- and fire-resistance) compared to OPC benchmarks [2–4]. Early- and late-age durability is dependent on a variety of processing factors, such as precursor chemistry, precursor blending, water-to-binder ratio, activator dose, and composition, and curing regime [5,6].

Recent research interest in reducing the environmental impact and improving the performance (*i.e.*, compressive strength) of OPC has led to the use of magnesium oxide (MgO) as a cement supplement [7] as well as the development of Mg-rich cementitious binders for various applications such as nuclear waste immobilization [8], precast construction, and road repair [9]. Study of M-S-H and other Mg-containing binders has garnered interest due to the buildup of Mg at interfaces between cement and natural rocks [10]. Brucite (Mg hydroxide) forms early in the synthesis of M-S-H, which dissolves as M-S-H is slowly formed [10,11]. The structure of M-S-H is often regarded as being phyllosilicate-like [8,12] with octahedral Mg and tetrahedral Si in alternating sheets [13]. Serpentine (*i.e.*, lizardite, antigorite, chrysotile) and phyllosilicate (*i.e.*, sepiolite, saponite, talc) mineral groups have been reported to be linked with M-S-H binders [9,14]. M-S-H binders usually exhibit a main ²⁹Si resonance peak at -97.7 ppm with downfield chemical shifts due to the deshielding effect of Mg ions (*i.e.*, increased Mg:Si ratios) [8]. The resultant structure is dissimilar from C-S-H in that M-S-H contains more chemically bound water and is generally organized in silicate sheets, rather than silicate chains [15].

The addition of Al in the synthesis process results a M-A-S-H binder, where Al substitutes both tetrahedra and octahedra in the phyllosilicate structure [13]. In the presence of Mg, Al also forms hydrotalcites or layered double hydroxide (LDH) phases [16,17] which are distinct from the binder but offer advantageous properties such as added carbonation resistance [18]. Recent syntheses and characterization of M-(N)-A-S-H binders indicate the possibility of Al incorporation in tetrahedral sheets layered with octahedral Mg sheets [19]. This study suggested that the structure is similar to clinocllore or

sepiolite phyllosilicates. These results suggest that interlayer molecules of water or OH groups are present between discontinuous octahedral layers.

In slag AAMs, the Mg content of the aluminosilicate precursors (approximately 7-10% MgO) is known to accelerate reaction kinetics and microstructure (*e.g.*, porosity, mineralogy) and strength development [20–22]. Bernard *et al.* have shown that after long time periods, low internal pH values of 9-10.5 are shown to form Mg aluminosilicate hydrate binders (M-A-S-H) with comparable polymerization degrees to M-S-H silicate sheets and limited coherent size [23]. Tetrahedral and octahedral Al sites were both observed in M-A-S-H, while no aluminum was present as an exchangeable cation on surface sites. Further research on the atomic structure of Mg-containing binder phases is important to deepen understanding of the long-term performance of cementitious materials as repositories for radioactive waste [24], as well as improving the CO₂ sequestration potential and durability of both MgO-additive cement and Mg-rich AAMs [25]. Moreover, little is yet known about phase assemblages in AAMs which are both low-Ca and Mg-rich.

In this work, sol-gel chemical principles were utilized to produce stoichiometrically-controlled Mg-rich AAMs. The Pechini sol-gel process utilizes *in situ* chemical directing agents (*i.e.*, polymers) to chelate metal ligands into a network. The polymeric component can be removed with calcination to yield a homogenous, multicomponent, single-phase, mixed metal oxide powder [26,27]. Since its inception, variations of the Pechini process frequently utilize poly(vinyl alcohol) (PVA) or poly(ethylene glycol) (PEG) as directing agents in solution with nitrate salts to synthesize mixed metal-oxide powders [28–32]. The chelation mechanism co-occurs while metal cations are sterically entrapped by the polymeric network [30–32]. Hence, this process is often named “organic steric entrapment.” In this study, the process is named polymer-assisted sol-gel synthesis (PASOG) to reflect its connection to traditional sol-gel processes. This method provides significant advantages when compared to traditional methods of producing AAMs. First, the method has been utilized in the production of high-purity geopolymer precursors [33–35] and OPC phases [36]. Second, dissolution kinetics closely resemble those in the alkali activation of industrial

byproducts [34]. Resultant stoichiometrically-controlled cementitious materials can therefore be leveraged to relate nanostructure of pure phases to durability properties.

Building upon recent findings on M-S-H binders, the primary objective of this study is to understand the atomic structure and phase assemblage of Ca-free, Mg-rich AAMs. Specifically, M-(N)-A-S-H AAMs were produced for the first time using the PASOG synthesis method and subsequently analyzed. It is hypothesized that altering experimental parameters of PASOG synthesis will produce distinct nanostructural features (*e.g.*, extent of crosslinking), as reported in previous work by the authors [37].

2. Materials and Methodology

2.1 Materials

The materials utilized to synthesize M-(N)-A-S-H cementitious materials *via* the PASOG method were aqueous SiO₂ suspension (LUDOX® HS-40 colloidal silica, Sigma Aldrich); poly(vinyl alcohol) (PVA, 98% hydrolyzed, Sigma Aldrich); poly(ethylene glycol) (PEG, 98% hydrolyzed, Sigma Aldrich); magnesium nitrate hexahydrate (Fisher Chemical, 98-102%); and, aluminum nitrate nonahydrate (Fisher Chemical, 99%). Nitrate salts were stored under vacuum to prevent intrusion of atmospheric water. A mineral oil (light paraffin oil, Fisher Chemical) bath was used to ensure constant synthesis temperatures. Aqueous sodium hydroxide (NaOH) (BioUltra, 10M, Sigma Aldrich) was utilized for alkali-activation. Plastic molds (14mm diameter cylindrical polyethylene vials, Electron Microscopy Sciences) were employed for casting, and a super-saturated sodium phosphate solution (96%, Sigma Aldrich) was used to achieve high relative humidity conditions (RH 99%) during curing [38]. Lastly, ethanol (anhydrous, 200 proof, Fisher Chemical) was used to dehydrate the resulting materials.

2.2 Methodology

2.2.1 Synthesis of Mg-aluminosilicate precursors

Four AAM precursors were synthesized using the PASOG method as described by Walkley *et al.* [33]. First, a polymeric solution of 5 wt% was prepared according to **Table 1** by dissolving the polymer (PVA or PEG) in deionized water at 70°C. The amount of polymer added was controlled to achieve a metal-to-oxygen ratio (M^+/O) of 2.0. In this ratio, a metal is an aluminum or Mg cation, whereas an ‘oxygen’ may be either an alcohol unit in PVA polymers or an ether unit in PEG polymers. The temperature was controlled with a mineral oil basin heated by a Corning™ Digital Hotplate and Stirrer in which reaction vessels were partially submerged. After complete polymer dissolution, 40 wt% aqueous Mg nitrate hexahydrate was added and allowed to mix for thirty minutes before adding 40 wt% aqueous aluminum nitrate nonahydrate. After another thirty minutes of mixing, 40 wt% aqueous suspension SiO_2 was added. During mixing, solutions were kept at 70°C and covered with aluminum foil to prevent excessive water evaporation. After mixing, the temperature was increased to 75°C and uncovered to permit the formation of a xerogel through a dehydration process for up to 48 h. Reaction vessels were subsequently removed from heat upon the appearance of a viscous, aerated xerogel. Mixtures containing PVA produced a dark yellow gel, whereas mixtures containing PEG produced a cloudy white gel. These precursor gels were then calcined at 550°C (for PVA-prepared materials) and 900°C (for PEG-prepared materials) according to [33] with a ramp rate of 3°C/min and a hold time of 1 h.

Table 1. M-(N)-A-S-H materials produced *via* the PASOG method and mass compositions.

Material	Polymer	Polymer MW (kDa)	Material properties		Chemical composition (%) [*]			
			M^+/O	L/S	SiO_2	Al_2O_3	MgO	Na_2O
L-PVA	PVA	13-23	2.0	1.0	24.0	12.5	14.4	15.2
H-PVA	PVA	31-50	2.0	1.0	23.1	13.9	16.2	13.5
L-PEG	PEG	20	2.0	1.0	29.5	15.6	18.4	14.0
H-PEG	PEG	35	2.0	1.0	27.4	13.7	16.4	17.3

^{*} Values obtained from ICP-OES Mg:Si ~1.0, Na:Al = 1.5-2.0, Si:Al= 1.5.

2.2.2 M-(N)-A-S-H AAM preparation

Calcined precursors were manually ground to pass a #100 sieve (150 μm) and mixed with aqueous NaOH in observance of liquid to solid ratios (L/S) in **Table 1**. Each mixture contained the same mass of precursor. Mixtures were stirred then poured into identical molds that were lubricated with VaselineTM to allow removal after curing. Filled molds were tapped on a flat surface for 10 s each to remove entrapped air, then cured at 35°C and 99% relative humidity (RH) for 24 h. 99% RH was achieved by placing molds in a sealed container with a supply of deionized water which was reacted with sodium phosphate according to ASTM E104. After humid curing, cementitious material materials were dried at 40°C for a minimum of 48 h before dehydration with ethanol and subsequent characterization. The chemical composition of resultant AAMs were determined with ICP (see **Table 1**) and agree well with typical slag-based AAM compositions as reported in [39].

2.2.3 Practical considerations

Previous PASOG studies have utilized PEG exclusively for the production of calcium-aluminosilicate precursors and PVA exclusively for the production of aluminosilicate precursors due to difficulties with sample retrieval, as described in [33]. These difficulties were not encountered in the current study. Additionally, previous studies have claimed negligible effects of the L/S ratio on precursor dissolution [34]. Considering such a claim, the authors explored using L/S=2.0 during activation. Mixtures of L/S=2.0 remained liquid whereas mixtures with L/S=1.0 formed semi-solid materials immediately upon activation and solidified completely after curing at elevated temperatures. These results suggest that L/S ratio may play an important role on precursor dissolution and formation of the Si-O-Al aluminosilicate binder network. L/S= 2.0 mixtures were not characterized further.

Methodological variables (calcination temperature, polymer type, and polymer molecular weight) impacted AAM structure. Temperature variations in calcination procedure (performed according to [33]) may have impacted the reactivity of synthetic AAM precursors [40]. However, a comprehensive study of this impact was not within the scope of this work. XRD results show that majorite results exclusively from PVA preparation and the polymorph enstatite exclusively from PEG. NMR and FTIR results showed that

increasing polymer molecular weight in the PASOG method resulted in elevated formation of extra-framework phases. The presence of octahedral Al as verified by ^{27}Al NMR [41,42] as well as FTIR [43–45] evinces extra-framework Al. Integration of ^{27}Al NMR peaks indicated that octahedral Al comprised a higher fraction of Al environments with the use of PEG, and in general with increasing molecular weight. Additionally, the H-PEG material is the only AAM of the four to have isolated Si (Q^0 Si environment, as shown in **Figure 1**). PEG-prepared AAMs possess higher variability of Si-O-T (where T = tetrahedral Al or Si) infrared vibrational modes relative to PVA-prepared AAMs, indicating a lower extent of cross-linking. Finally, the content of physisorbed water (quantified using ^1H - ^{29}Si and ^1H - ^{27}Al CP MAS NMR and TGA/DTG) was lower in PEG-prepared AAMs. Thus, using PEG rather than PVA in PASOG synthesis, as well as increasing either polymer molecular weight, results in higher concentration of extra-framework phases, an expected decrease in cross-linking, and higher chemical shrinkage. These results are consistent with findings of Gevaudan *et al.* for synthetic geopolymers (*i.e.*, N-A-S-H) where PVA polymers were preferential for PASOG synthesis of cementitious binders [37]. Lastly, all materials demonstrate alkane and nitrate vibrations discovered by FTIR (see assignments in **Table 2**). These are respectively attributable to polymers and nitrate-based salts used during the PASOG method which were not successfully removed during calcination.

Full characterization of structural variability resulting from PASOG methodological differences is beyond the scope of this work. Instead, the authors pursue an analysis of the similarities between structures in alkali activated slags and this work's novel, calcium-free, Mg-rich AAMs.

2.3 Material Characterization

2.3.1 ^{29}Si , ^{27}Al and ^{23}Na Solid-State Magic-Angle Spinning Nuclear Magnetic Resonance Spectroscopy (^{29}Si , ^{27}Al , and ^{23}Na MAS NMR)

To characterize atomic structures, solid-state ^{29}Si , ^{27}Al , and ^{23}Na MAS NMR spectra were acquired using a Varian INOVA 400 MHz NMR spectrometer (magnetic field 9.39 T; an operating frequency of 79.50 MHz for ^{29}Si , 104.27 MHz for ^{27}Al , and 105.85 MHz for ^{23}Na). Samples were packed into 4 mm zirconia rotors

sealed at either end with Teflon plugs, and all spectra were collected with magic-angle spinning (MAS) speed of 10 kHz using a broadband probe equipped with a 4 mm MAS module designed and manufactured by Revolution NMR, LLC (Fort Collins, CO). All experiments (Bloch-decay as well as cross polarization for all nuclei) utilized a 90° pulse angle. ^{29}Si chemical shifts were determined using a reference of DSS (2,2-dimethyl-2-silapentanesulfonate) at 1.46 ppm. The spectra were acquired through a Bloch-decay experiment with 1600 scans using a pulse recycle delay of 45 s, a pulse width of 4.5 μs , and an acquisition time of ~ 20 ms. ^{27}Al chemical shifts were referenced to aluminum nitrate ($\text{Al}(\text{NO}_3)_3$) at 0 ppm and the Bloch-decay experiment was acquired using a pulse recycle delay of 5 s, a pulse width of 4.0 μs , an acquisition time of ~ 30 ms, and 256 scans. ^{23}Na chemical shifts were determined using a NaCl reference at 0 ppm. The Bloch-decay experiment was acquired using a pulse recycle delay of 5 s, a pulse width of 5.25 μs , an acquisition time of ~ 20 ms, and 256 scans. Cross-polarization (^1H - ^{29}Si CP) MAS NMR data were also collected using ^1H and ^{29}Si pulse widths of 3.8 and 4.5 μs respectively with recycle delay of 3 s, CP spin-lock time of 3 ms, and 2048 scans. For ^1H - ^{27}Al CP MAS NMR experiments, ^1H and ^{27}Al pulse widths of 3.8 and 4.0 μs , respectively, were used with a recycle delay of 2 s, CP spin-lock time of 2 ms, and 256 scans.

Analysis of the collected data was performed using MestreNova 11.0 software. Peak deconvolution was not attempted due to low signal to noise ratio. However, literature with NMR data for M-S-H, M-A-S-H, and (C,N)-A-S-H AAMs were compared to provide a qualitative understanding of results [13,16,17,23,35,46–49].

2.3.2 Fourier transform infrared spectroscopy (FTIR)

Nanostructure was further characterized using FTIR. Samples for analysis were ground and homogenized by hand. Next, 0.020 ± 0.001 grams of each sample were mixed with 2.000 ± 0.100 grams of potassium bromide (KBr) spectrograde powder (International Crystal Labs). Thus, KBr disk sample concentration was 1 wt%. Mixtures were homogenized in a Spex Grinder mill to ensure uniform particle size. This is important to reduce peak intensity differences. Solid KBr sample mixes were pressed into KBr disk pellets

for analysis in a Thermo Scientific Nicolet iS10 FTIR Spectrometer. Disks were analyzed against a blank background to remove the absorption spectra from the nitrogen-purged chamber. Increased intensity of the H-PVA FTIR spectrum relative to other spectra (see **Figure 4**) is likely a result of sample error due to increased localized concentration gradients within the KBr pellet.

2.3.3 X-ray diffraction (XRD)

Materials were crushed with a mortar and pestle and subsequently well-packed in XRD sample holders to determine the mineralogy of M-(N)-A-S-H AAMs. The method was modified to employ corundum as an internal standard instead of zincite. Diffraction patterns were acquired using a Siemens D500 X-ray diffractometer. Samples were analyzed from $2\theta = 5^\circ$ to 65° using Cu $K\alpha$ X-ray radiation, with a step size of 0.02 degrees and a dwell time of two seconds per step. Mineralogy was identified using Jade software (MDI, Version 9) and the International Centre for Diffraction Data (ICDD) 2003 database.

2.3.4 Thermogravimetric analysis and differential thermogravimetry (TGA/DTG)

Material water content and volatiles composition were determined by analyzing powdered samples of ~50 mg in an Al_2O_3 crucible using a Netzsch STA. A heating rate of $3^\circ C/min$ between room temperature ($25^\circ C$) and $1000^\circ C$ in air purged chamber at 70 standard cubic centimeters per minute (SCCM) plus argon purged at 20 SCCM were utilized. Mass differentials were determined as sample burn-off occurred. Determination of the rate of mass change with respect to temperature (differential thermogravimetry or DTG) was performed using the 'Differentiate' function of mass with respect to temperature data in OriginPro 2018.

2.3.5 Inductively Coupled Plasma – Optical Emission Spectrometry (ICP-OES)

A commercial laboratory (Hazen Research, Inc., Golden, CO) was employed to perform a chemical characterization of the materials. A Perkin Elmer Optima 7300DV with a dual view was utilized to perform the chemical analysis of the materials. Prior to analysis, sample aliquots weighing between 0.10-0.20 g were added to a 95%/5% Pt/Au crucible containing 2 grams flux (1:1 lithium metaborate/lithium tetraborate). The sample was mixed, and then 5-10 drops of 25% lithium bromide were added. Next, acid

digestion was performed in a Teflon beaker placed on the Claisse fusion stirrer, with ~90 mL of DI water, 10 mL of concentrated hydrochloric acid and 1 mL of concentrated hydrofluoric acid. Subsequently, the contents of the crucible were fused using the Claisse fusion program and then poured into a waiting beaker before ICP-OES. In order to ensure the accuracy of the results, a basalt standard was also submitted to analysis. It was found that the oxide composition reported had a ~1.0% oxide error.

2.3.6 Chemical Shrinkage

Chemical shrinkage is reported as percent change from the inner diameter of the plastic mold to the measured material diameter after curing, drying, and dehydration. Using calipers, material diameters were arithmetically averaged from six points along the cylindrical material to the nearest 0.01 mm.

3. Results and Discussion

3.1 Atomic and Molecular Structure of M-(N)-A-S-H AAMs

PVA-prepared M-(N)-A-S-H materials exhibit main and broad resonances indicating Q^2 silicate tetrahedra (-86 ppm) and possible Al and Mg incorporation into the silicate structure (-90 ppm, -93 ppm); while PEG-prepared M-(N)-A-S-H materials exhibit less connected (-80 ppm) and non-connected silicate structures (-70 ppm). As shown in **Figure 1a**, L-PVA and H-PVA materials exhibit ^{29}Si NMR signals in the range of -80 to -92 ppm, while L-PEG and H-PEG materials exhibit downfield chemical shifts in the range of -70 to -86 ppm. Previous PASOG work by the authors shows calcined SiO_2 precursor materials with resonances at -110 ppm [37]. The absence of such resonances indicates highly reactive synthesized precursors. The broad ^{29}Si resonance peak observed for both PVA materials at -86 ppm (Q^2) is more shielded than those found in traditional M-S-H binders (peak at -85 ppm) [13]. These differences reveal slight modifications to the silicate structure, possibly due to Al substitution. Furthermore, the hump between -82 ppm ($Q^2(1\text{Al})$) and -80 ppm (Q^1), has not been reported in previous M-S-H binder studies, and may represent middle- and end-chain units in incomplete or disordered silicate sheets as reported recently in M-A-S-H and M-(N)-A-S-H binders [13,19]. The atomic structures of M-(N)-A-S-H characterized herein indicate the presence of

highly shielded signals near -92 ppm likely due to the presence of Q^3 sites, as similarly observed in M-S-H [23]. By considering the assignment of peaks at -80 ppm and -86 ppm, as well as the chemical shift by $Q^n(mAl)$ units and upfield peaks, ~ -92 ppm can also be assigned to $Q^4(3Al)$. Furthermore, the signal near -89 ppm evinces a $Q^4(4Al)$ site [37]. These assignments suggest a high degree of Al substitution in the silicate sheet, resulting in an interconnected Si-Al network. Such a hypothesis is supported by recent characterization of M-(N)-A-S-H materials with X-ray absorption near-edge spectroscopy [19]. Contrastingly, PEG-prepared materials exhibit chemical environments dominated by Q^1 atomic sites, indicating a less connected silicate structure. Moreover, the peak at -70 ppm indicates a non-connected (Q^0) silicate [50–53].

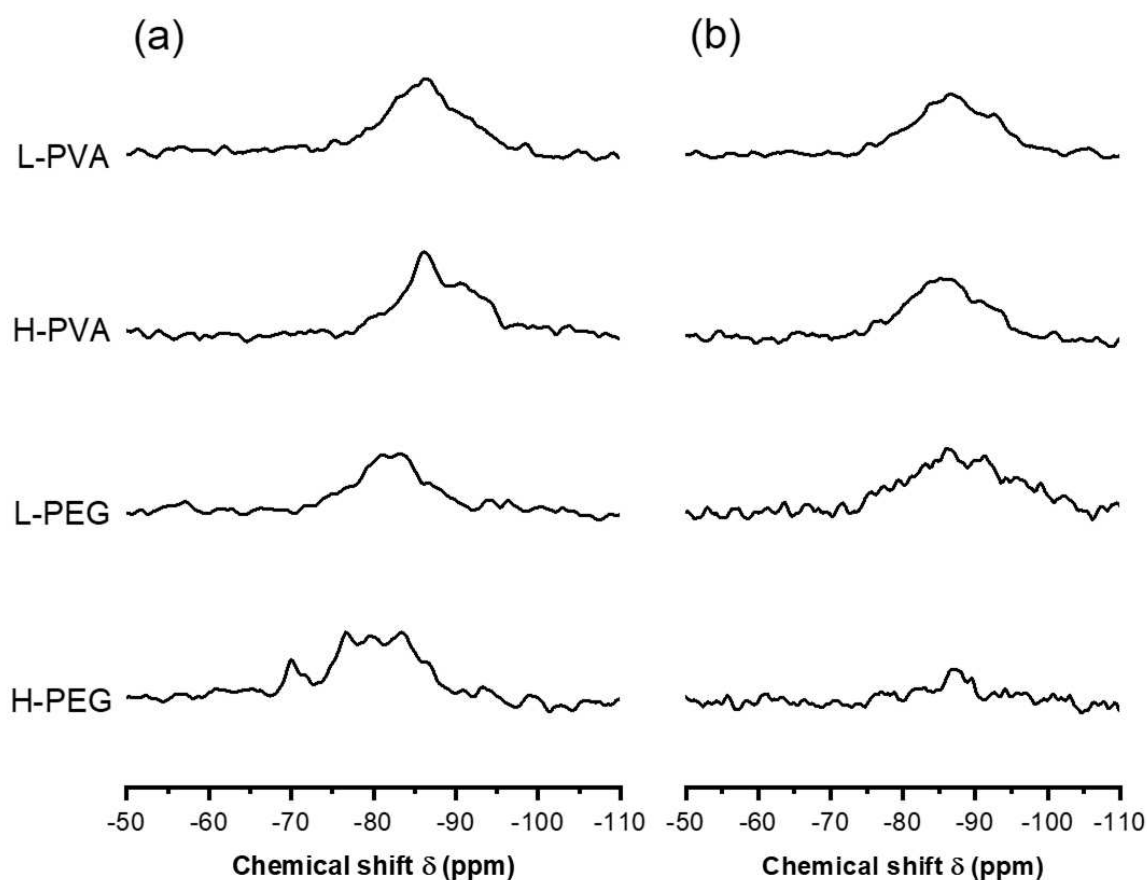


Figure 1. (a) ^{29}Si DP and (b) 1H - ^{29}Si CP NMR spectra of M-(N)-A-S-H AAMs.

The appearance of Q^2 resonances in ^{29}Si NMR indicates an incomplete or disordered silicate sheet. This hypothesis is further supported by the appearance of single peaks at -86ppm in **Figure 1b** which are assigned to Q^2 units with single silanols [16,47]. The presence of single silanols in Q^2 units is similarly found in amorphous aluminosilicates, silicates, and zeolites [37,54], as well as alkali-activated slags [16,17]. The presence of Q^2 single silanols (Si-OH) yields the formation of Si-O^- moieties, which are likely charge-balanced by cations (*i.e.*, Na^+ , Mg^{2+}) [16]. Resonances at -92 ppm in PVA-prepared AAMs may indicate $Q^3(\text{Mg})$ activity [55], which would be expected due to adjacent Si and Mg sheets in phyllosilicate-type materials [13]. Unlike alkali-activated slags, $^1\text{H-}^{29}\text{Si}$ CP does not enhance Q^1 terminal sites or Q^3 bridging sites, indicating that no near-field hydroxyls exist near these atomic coordinations. Lastly, the resonances found here may also indicate the presence of Si interactions with interlayer water resembling those found in the enstatite or preiswerkite/phyllosilicate phases [56,57]. Section 3.2 provides detailed discussion of mineralogy.

M-(N)-A-S-H materials contain Al(IV) (~60 ppm) and Al(VI) (10 ppm) atomic environments, which correspond to Al in tetrahedral and octahedral coordination in the binder structure as well as octahedral Al in Mg-Al layered double hydroxide (LDH) phases (**Figure 2a**). Paired with data from ^{29}Si NMR signals, specifically resonances at -82ppm (**Figure 1a**), it is further confirmed that PVA-prepared M-(N)-A-S-H materials contain Al(IV)-substituted silicates forming $Q^2(1\text{Al})$ sites. Furthermore, Al(IV) likely participates in cross-linked Q^3 or Q^4 sites within the tetrahedral silicate sheet of the binder. As similarly found for M-S-H binders, no NMR evidence confirmed the presence of Al(V) within these Mg-based materials to balance negatively charged moieties [46,48]. $^1\text{H-}^{27}\text{Al}$ CP resonances (see **Figure 2b**) further confirm the presence of Al(VI) with pendant hydroxyl units characteristic of Mg-Al LDH phases, which are likely intermixed with the atomic structure of the M-(N)-A-S-H binder as similarly observed for alkali-activated slags [58]. Evidence for the creation of Mg-Al LDH phases is an innovative result, as recent findings on Al-substituted M-S-H materials were not able to achieve necessary saturation conditions during

activation to observe their formation [13,59,60]. Further evidence of these phases will be discussed in later sections with regards to the phase assemblage of M-(N)-A-S-H materials.

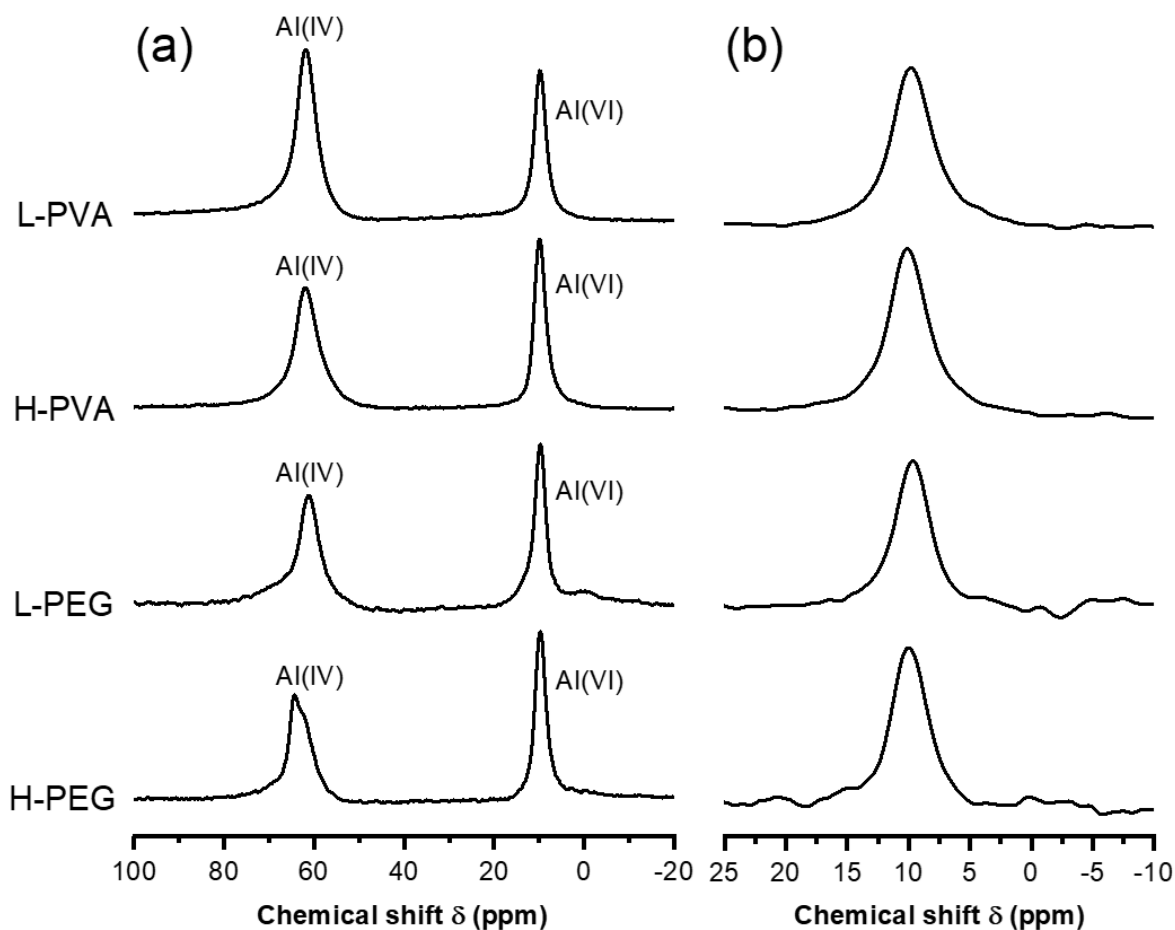


Figure 2. (a) ^{27}Al DP and (b) ^1H - ^{27}Al CP NMR spectra of M-(N)-A-S-H AAMs.

^{23}Na NMR spectra are usually broadened by quadrupolar interactions and sometimes featureless due to structural disorder. Linewidth of ^{23}Na is sensitive to the local Na coordination environment (H_2O or OH) due to change in the vibrational energy of Na motions., ^{23}Na NMR resonances demonstrate that M-(N)-A-S-H contains hydrated Na ions in their binder structure ($\delta_{\text{Na}} = -20$ ppm) (see **Figure 3**) [35,49]. The broad resonance in PEG-prepared materials (-40 ppm to 0 ppm) in comparison to PVA-prepared materials may be due to the combination of variably coordinated Na^+ in the system, quadrupolar effects and variable Si- Na^+ interactions. The presence of the Q^0 in ^{29}Si NMR in addition to Q^2 and Q^3 species confirms the

presence of multiple crystalline Si sites in PEG-prepared materials [61–63]. In addition, the peak from -40 ppm to -20 ppm can be assigned to the Na_2CO_3 (Natrite) species discussed in further detail in Section 3.2. Contrastingly, PVA-prepared materials exhibit narrow ^{23}Na NMR peaks with fewer resonances of comparable intensities which indicates the presence of more homogeneous Na sites or coordination states in comparison to PEG-prepared materials [61–63]. Although **Figure 3** provides a qualitative overview, two dimensional or multiple quantum experiments would be needed to make more definitive assignments of these features, which is beyond the scope of this study.

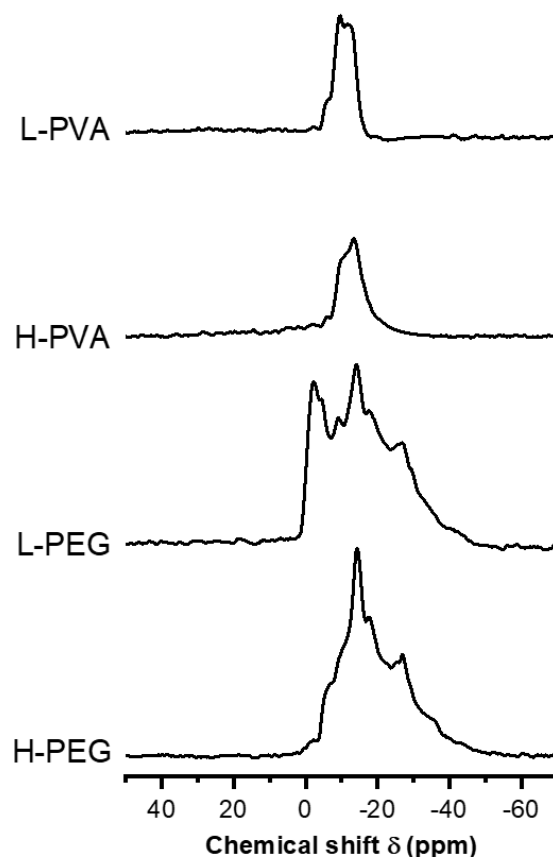


Figure 3. ^{23}Na MAS NMR direct-polarization spectra of M-(N)-A-S-H AAMs.

FTIR results are presented in **Figure 4**. Silicate bands characteristic of M-S-H materials are observed between $870\text{--}920\text{ cm}^{-1}$ and $950\text{--}1150\text{ cm}^{-1}$ [64]. Strong broad FTIR peaks at 1040 cm^{-1} and 460 cm^{-1} corresponding to Si-O-T stretching in cross-linked aluminosilicates provide additional evidence for Al

substitution in silicate sheets [65–67], see **Figure 4** and **Table 2**. These Si-O-T stretching bands appear at $\sim 990\text{ cm}^{-1}$, and an increase in wavenumber is associated with a higher degree of Al substitution [65]. As supported by the ^{29}Si and ^{27}Al NMR spectra, the Si-O-T band stretching here corresponds to the Si-O-Al substituted silicate sites within the M-(N)-A-S-H binder. Similar observations have been made for low pH M-A-S-H cementitious materials [13]. It is worth considering that these results are only evident in PVA-prepared materials, as PVA polymers enable efficient preparation of reactive phases as detailed by the authors in other work [37]. PEG-prepared materials result in phase segregation *via* $\text{AlO}_6\text{-AlO}_4$ interactions ($630\text{-}760\text{ cm}^{-1}$) and separation of silicates, as evidenced by Si-O-Si bonds ($400\text{-}500\text{ cm}^{-1}$) [43,44,65,67–72]. Unexpectedly, octahedral Al-O vibrations in the H-PEG FTIR spectrum were not discernible. These data provide evidence that PVA is more appropriate than PEG to use in PASOG synthesis of M-(N)-A-S-H. In subsequent sections, PEG-prepared materials will be presented for completion.

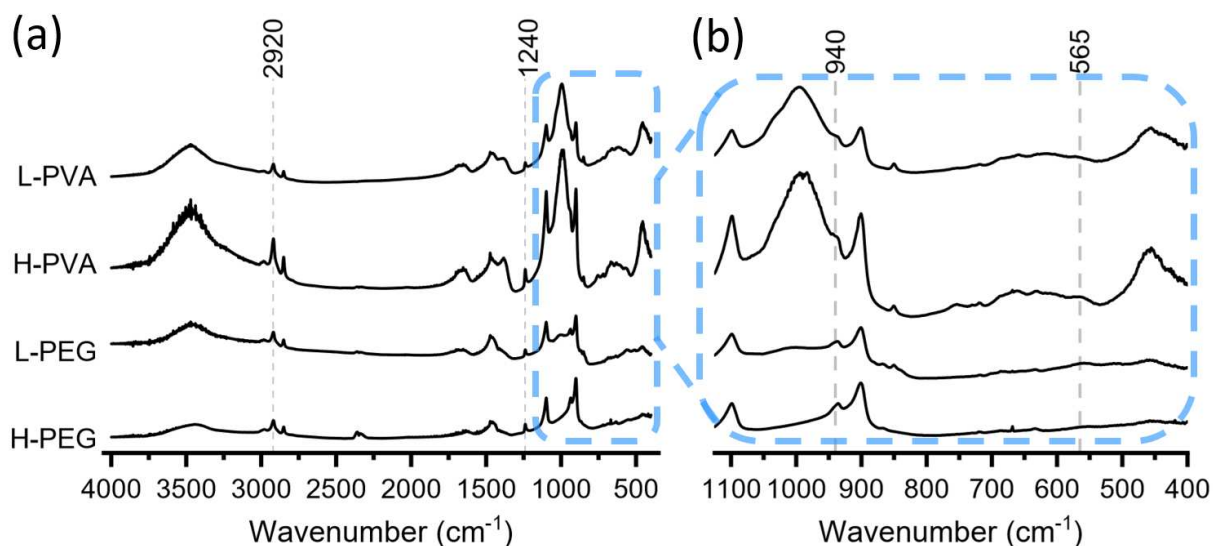


Figure 4. (a) FTIR spectra of M-(N)-A-S-H AAMs and (b) expanded spectra from $1150\text{-}400\text{ cm}^{-1}$.

Table 2. Summary of FTIR results. Shaded box indicates band appearance in respective material. (s) = strong, (sh) = shoulder, (w) = weak, (t) = trace.

Wavenumber (cm ⁻¹)	Assignment	L-PVA	H-PVA	L-PEG	H-PEG	References
3740	O-H stretching		(w)	(w)	(w)	[73]
3800-3200	O-H stretching	(s)	(s)	(s)	(s)	[74,75]
2980	C-H stretching	(w)	(w)	(w)	(w)	[76]
2920	CH ₂ -CH ₂ asymmetric stretching	(s)	(s)	(s)	(s)	[77,78]
2850	CH ₂ -CH ₂ symmetric stretching	(s)	(s)	(s)	(s)	[77,78]
1655	O-H bending	(s)	(s)	(s)	(s)	[74,75]
1470	C-O stretching	(s)	(s)	(s)	(s)	[72]
1380	C-O stretching	(s)	(s)			[79,80]
1240	N-O stretching	(s)	(s)	(s)	(s)	[81]
1100	Si-O-Si stretching	(s)	(s)	(s)	(s)	[68–71,82,83]
1050-950	Si-O-T (T = Al or Si) stretching	(s)	(s)	(w)		[65–67]
1030	Si-O-T (T = Al or Si) stretching	(sh)				[65–67]
940	Si-OH stretching	(sh)	(sh)	(s)	(s)	[71,82–86]
900	Si-O-Si stretching	(s)	(s)	(s)	(s)	[75,82,83,87]
865	SiO-H bending			(w)	(w)	[82,83,88]
850	SiO-H bending	(s)	(s)	(s)		[82,83,88]
755	Various TO ₄ -TO ₄ vibrations (T = Al or Si); AlO ₄ -AlO ₆ interaction vibrations		(w)			[43,44,65,67,69,72,89]
720			(w)	(t)	(t)	
685		(w)	(w)			
670			(t)	(t)	(w)	
660		(w)	(w)			
635			(w)	(w)	(w)	
570-560	Al-O stretching	(t)	(w)	(w)		[43–45]
500-400	Si-O-Si and O-Si-O bending	(s)	(s)	(w)	(t)	[67–71,84,88]

3.2 Phase assemblage of M-(N)-A-S-H AAMs

As observed in **Figure 5**, M-(N)-A-S-H materials form zeolite phases, such as sodalite and zeolite Y, which can nucleate from regions of the binder resembling N-A-S-H. More specifically, PVA-prepared materials contain sodalite carbonate– zeolites with carbonate enclathrated within the sodalite cage [90]. Additionally, the L-PEG material contains a sodium aluminosilicate hydrate mineral with a comparable structure to zeolite Y [91]. The presence of zeolites is expected from alkali-activation of aluminosilicates using the processing and curing methods employed herein [92–94]. As previously discussed for PVA-prepared M-(N)-A-S-H materials, the ^{29}Si NMR assignment of $\text{Q}^4(3\text{Al})$ and $\text{Q}^4(4\text{Al})$ (**Figure 1a**) indicates that part of the M-(N)-A-S-H structure may resemble recently proposed atomic structural models of N-A-S-H binder [37,95]. This assignment is consistent with the formation of zeolites observed in low-calcium activated precursors (*e.g.*, metakaolin).

As supported by Al(VI) NMR resonances, the formation of Mg-Al LDH phases can be observed in **Figure 5**. The Mg-Al LDH phase meixnerite appears to form in H-PVA and H-PEG M-(N)-A-S-H, and trace meixnerite peaks are also present in the L-PVA XRD pattern. The formation of Mg-Al LDH phases is expected due to high pH during activation, which permits the achievement of super-saturated conditions favorable for Mg-Al precipitation [13]. The presence of these phases regardless of PVA or PEG preparation indicates that their formation is only dependent on these ions achieving sufficient super-saturation conditions during activation – an important finding for the production of these phases and improving the material’s durability. For example, the presence of LDHs is known to counteract carbonation by atmospheric CO_2 and prevent strength loss, as previously reported by [18] in alkali-activated slags. Furthermore, these phases can impart other durability benefits, as they can reduce chloride permeability in cementitious materials [96].

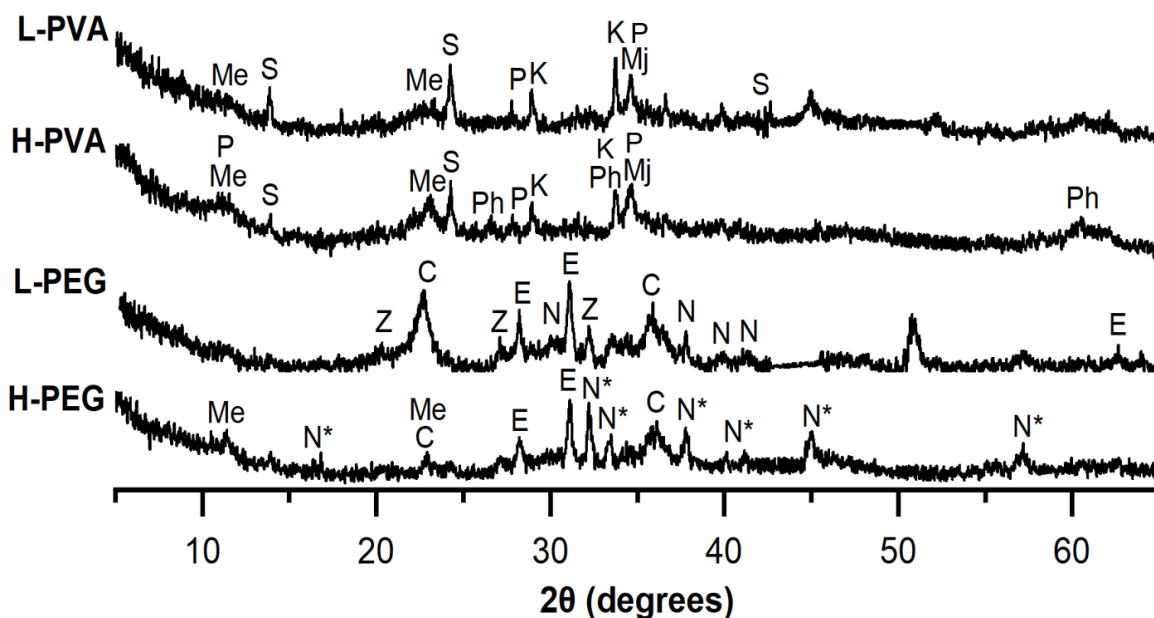


Figure 5. X-Ray Diffraction Patterns for all M-(N)-A-S-H AAMs. C = Sodium Magnesium Aluminum Silicate (00-049-0008), E = Enstatite (00-019-0768), K = Kornerupine (01-074-1394), Me = Meixnerite (00-050-1684), Mj = Majorite (00-047-1750), N = Natrite (00-037-0451), N* = Sodium Carbonate Hydrate (01-070-2148), P = Preiswerkite (01-082-0039), Ph = Sodium Phlogopite (00-027-0731), S = Sodalite (00-049-0757), Z = Zeolite Y (00-043-0168).

Preiswerkite and sodium phlogopite appear in PVA-prepared M-(N)-A-S-H materials, whereas PEG-prepared materials exhibit a distinct sodium magnesium aluminosilicate (denoted as C in **Figure 5**), which is proposed to be an Mg-containing modified β -cristobalite [97]. Preiswerkite and phlogopite are magnesium sodium aluminosilicates belonging to the phyllosilicate mineral group [98], [57]. Other phyllosilicates such as sepiolite and talc have been previously associated with formation of M-S-H [9]. Preiswerkite and phlogopite are 1M polytype trioctahedral micas with similar structures but variable structural flexibility. Seminal research on preiswerkite has revealed that Mg, Si and Al substitutions yields considerable ditrigonal distortions of the tetrahedral sheets and a decrease in the octahedral dimensions with interlayer sites occupied by Na [57]. ^{23}Na NMR (**Figure 3**) confirms the presence of hydrated Na^+ in these M-(N)-A-S-H AAMs. The high degree of Al substitution confirmed by NMR and FTIR data results in partial ordering of the octahedral sites and limitation of long range order. Lack of long range order is in line with the amorphous character of the XRD data (**Figure 5**) and broad ^{29}Si resonances (**Figure 1**). These

results have also been confirmed for other nano-porous phyllosilicates (*e.g.*, sepiolite) which are easily amorphized by dehydroxylation and grinding. These amorphized minerals reveal broad resonances at \sim -90 ppm with a shoulder discernible at -87 ppm [99]. Similarly, the presence of preiswerkite and phlogopite in both PVA-prepared M-(N)-A-S-H materials can explain observed resonances at -90 ppm and -93 ppm which resemble those often observed in geopolymers. These results signify that partly-amorphous minerals contribute to a material with characteristics analogous to those of traditional aluminosilicate geopolymers.

The atomic structure of M-(N)-A-S-H binders is partly amorphous and includes a tetrahedral layer of Si and Al and an octahedral layer of Mg, with Na⁺ most likely in the interlayer position. This work's evidence for Al substitution in tetrahedral Si sheets supports results from recent studies of M-(N)-A-S-H materials [19]. Atomic structures herein resemble sepiolite, preiswerkite, and phlogopite, which are all poorly crystalline phyllosilicates with continuous tetrahedral sheets and discontinuous octahedra [99]. Additionally, the presence of MgSiO₃ structures (*i.e.*, enstatite, majorite) provides additional evidence for M-S-H type phases [100,101]. Lastly, alkali-activation of PEG-prepared materials led to the formation of sodium carbonate phases, indicating poor extent of activation of the precursor. Excess sodium is susceptible to reaction with ambient CO₂ as found by the authors in other work [37].

3.3 Analysis of the hydrated structure of M-(N)-A-S-H materials

Molecular structural studies of M-(N)-A-S-H identified the presence of O-H bonds and hydrated Al(OH) and Q² Si-OH species (**Figure 2**, **Figure 4**). FTIR evidence corresponding to O-H stretching in water [74,75] and O-H bending vibrations of both free and chemically bound water [74,75] are indicated by broad bands at \sim 3500 cm⁻¹ and the double-peak at \sim 1660 cm⁻¹, respectively. TGA data confirm the presence of hydroxyl units recently characterized in M-A-S-H binders with a mass loss between 250°C and 700°C, constituting structurally bound water of hydrated phases [13]. As indicated by the mass loss between 0-100°C reported in **Table 3** [102–104], M-(N)-A-S-H materials lose about 10% of their mass due to evaporation of loosely bound water, as similarly reported in recent literature [13,59]. Unlike its M-S-H and M-A-S-H binder counterparts, M-(N)-A-S-H reveals distinct DTG peaks at 300°C and 600°C with no

formation of brucite (*i.e.*, $\text{Mg}(\text{OH})_2$) which would be marked by a mass loss at 400°C [13,60,64]. These peaks correspond to dehydroxylation and may be associated with the dehydroxylation of aluminols and silanols [102,104], as well as Mg-Al LDHs [105]. Dehydroxylation was higher in PVA-prepared materials (37-39% of total mass loss) than PEG-prepared materials (23-25% of total mass loss). Dehydroxylation near 600°C appears to occur at slightly higher temperatures for PVA- than PEG-prepared materials indicating either (1) an increase of extra-framework cation concentration or (2) a higher degree of Al substitution. Both of these effects are known to result in slower water desorption (*i.e.*, mass loss at increasingly higher temperatures) [105,106].

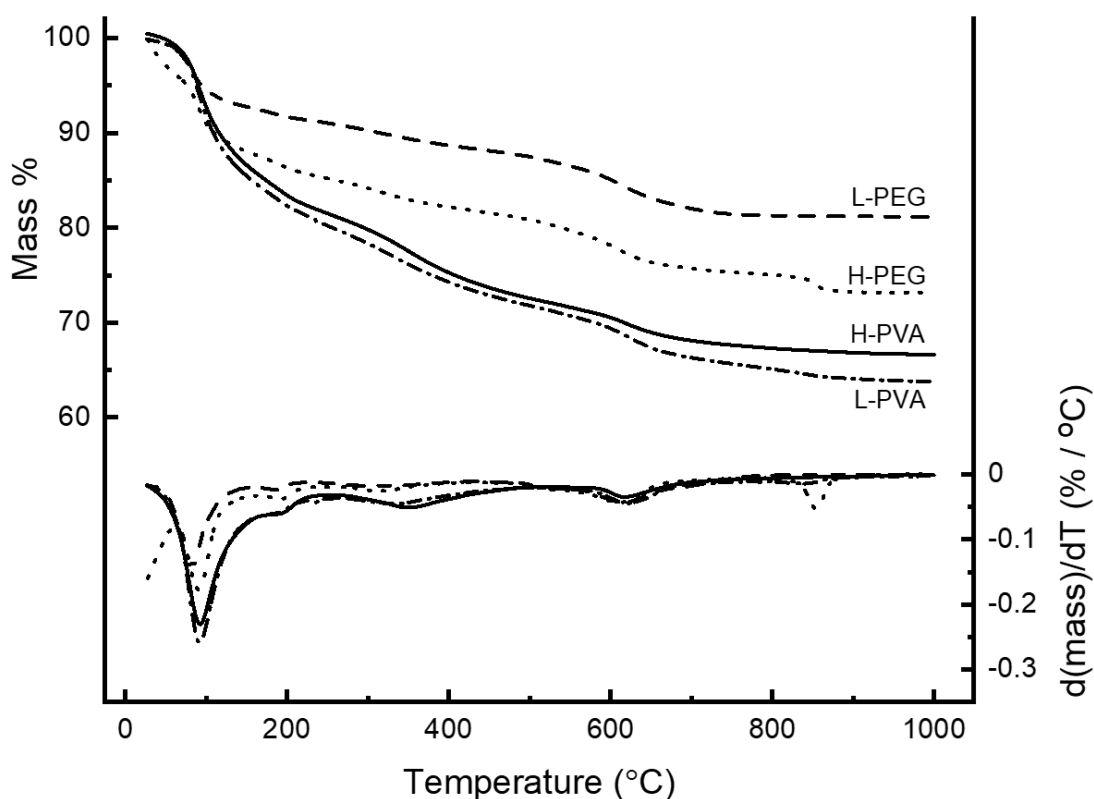


Figure 6. TGA and DTG curves for all M-(N)-A-S-H materials.

Table 3. TGA summary. Mass loss from $0\text{--}100^\circ\text{C}$ is attributable to free and loosely physisorbed water, $100\text{--}300^\circ\text{C}$ to chemisorbed water, $300\text{--}700^\circ\text{C}$ to dehydroxylation, and $700\text{--}1000^\circ\text{C}$ to decarbonization.

Material	Total mass loss (%)	% of Total Mass Loss			
		0–100°C	100–300°C	300–700°C	700–1000°C
L-PVA	36.2	22.7	37.0	33.1	6.9
H-PVA	33.4	21.9	38.6	35.0	4.5
L-PEG	18.8	28.7	22.9	43.6	4.8
H-PEG	26.8	33.6	25.4	31.3	9.3

3.4 Chemical Shrinkage of M-(N)-A-S-H AAMs

Chemical shrinkage is the decrease in material volume with time that is independent of external action [107]. Chemical shrinkage occurs during the AAM curing process when pastes, mortars, and concretes are in an initial, plastic state [108]. As reported in **Figure 7**, chemical shrinkage is significantly lower for PVA-prepared M-(N)-A-S-H materials as a result of (1) higher Al-crosslinked atomic structure (Q^2 , $Q^3(1Al)$) in **Figures 1 and 2**); (2) higher Al incorporation in silicate sheets (Si-O-Al bonds in **Figure 4**); and, (3) higher content of chemically-bound structural water (**Figure 6**). In agreement with literature, greater extent of Al substitution in the M-(N)-A-S-H binder is correlated with lower chemical shrinkage (~2%). Moreover, M-(N)-A-S-H AAMs chemically incorporate structural water, which limits volume reductions associated with dehydration of Si-rich phases [38,109]. In PEG-prepared materials, the presence of extra-framework Si phases (Q^0 and Q^1 Si) are correlated with increased chemical shrinkage, as expected due to the loss of free pore water. Excessive shrinkage can result in cracking and lead to intrusion of aggressive agents (*e.g.*, chlorides, sulfates) and thus represents a significant factor for affecting early-age durability of M-(N)-A-S-H materials.

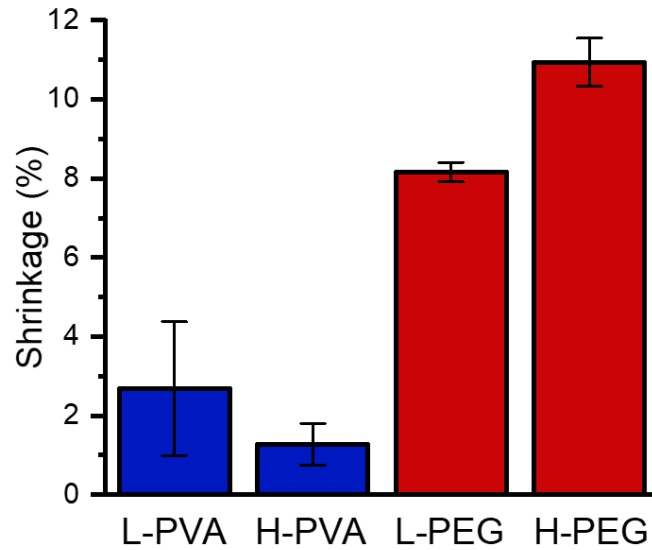


Figure 7. Chemical shrinkage for M-(N)-A-S-H AAMs. Error bars denote maximum and minimum values.

4. Conclusions

This study aimed to understand the atomic structure and phase assemblages in M-(N)-A-S-H AAMs produced by the alkali-activation of calcium-free, Mg-rich aluminosilicate precursors. The polymer-assisted sol-gel synthesis (PASOG) method was utilized to produce M-(N)-A-S-H AAMs. In accordance with previous research, it was found that PVA polymers were more effective than PEG polymers in producing Al-substituted M-(N)-A-S-H binders. Results extend upon recent investigations of M-(N)-A-S-H materials and demonstrate some similarity to more widely characterized M-S-H and M-A-S-H materials. The atomic structure of M-(N)-A-S-H is proposed to be a partly amorphous modified phyllosilicate with Si and Al tetrahedral sheets layered with Mg octahedral sheets and likely interlayer hydrated Na cations. This work demonstrates appreciable Al substitution within disordered tetrahedral silicate sheets, hydrated charge-balancing Na cations, and the formation of crystalline phyllosilicate phases such as preiswerkite and sodium phlogopite. In addition, activating conditions form mineral phases of interest such as Mg-Al LDHs (*i.e.*, meixnerite) as well as zeolites (*i.e.*, sodalite). TGA confirms the presence of hydrated phases and hydroxyls in M-(N)-A-S-H AAMs which are correlated with extra-framework (Q^0 and Q^1) Si phases and chemical shrinkage. This work contributes to the complexity of understanding regarding M-(N)-A-S-H and

exhibits palpable early- and late-age durability benefits, warranting further exploration of Ca-free, Mg-rich alkali activated materials.

5. Acknowledgments

This research was made possible by the Department of Civil, Environmental, and Architectural Engineering, the College of Engineering and Applied Sciences, and the Living Materials Laboratory at the University of Colorado Boulder. This work was supported by the National Science Foundation grant CBET-1604457. Dr. Kate Campbell and Mr. Tyler Kane of the United States Geological Survey (USGS) are gratefully acknowledged for their assistance with XRD. Dr. J.P. Gevaudan's participation to supervise, guide and complete this study was supported by the European Union's Horizon 2020 research and innovation programme under the Marie Skłodowska-Curie grant agreement No. 839436. This work represents the views of the authors and not necessarily those of the sponsors.

6. References

- [1] C. Le Quéré, R.M. Andrew, P. Friedlingstein, S. Sitch, J. Hauck, J. Pongratz, P.A. Pickers, J.I. Korsbakken, G.P. Peters, J.G. Canadell, A. Arneeth, V.K. Arora, L. Barbero, A. Bastos, L. Bopp, F. Chevallier, L.P. Chini, P. Ciais, S.C. Doney, T. Gkritzalis, D.S. Goll, I. Harris, V. Haverd, F.M. Hoffman, M. Hoppema, R.A. Houghton, G. Hurtt, T. Ilyina, A.K. Jain, T. Johannessen, C.D. Jones, E. Kato, R.F. Keeling, K.K. Goldewijk, P. Landschützer, N. Lefèvre, S. Lienert, Z. Liu, D. Lombardozzi, N. Metzl, D.R. Munro, J.E.M.S. Nabel, S. Nakaoka, C. Neill, A. Olsen, T. Ono, P. Patra, A. Peregon, W. Peters, P. Peylin, B. Pfeil, D. Pierrot, B. Poulter, G. Rehder, L. Resplandy, E. Robertson, M. Rocher, C. Rödenbeck, U. Schuster, J. Schwinger, R. Séférian, I. Skjelvan, T. Steinhoff, A. Sutton, P.P. Tans, H. Tian, B. Tilbrook, F.N. Tubiello, I.T. van der Laan-Luijkx, G.R. van der Werf, N. Viovy, A.P. Walker, A.J. Wiltshire, R. Wright, S. Zaehle, B. Zheng, Global Carbon Budget 2018, *Earth Syst. Sci. Data*. 10 (2018) 2141–2194. <https://doi.org/10.5194/essd-10-2141-2018>.
- [2] M. Sofi, J.S.J. Van Deventer, P.A. Mendis, G.C. Lukey, Engineering properties of inorganic polymer concretes (IPCs), *Cem. Concr. Res.* 37 (2007) 251–257. <https://doi.org/10.1016/j.cemconres.2006.10.008>.
- [3] P. Duxson, A. Fernández-Jiménez, J.L. Provis, G.C. Lukey, A. Palomo, J.S.J. Van Deventer, Geopolymer technology: The current state of the art, *J. Mater. Sci.* 42 (2007) 2917–2933. <https://doi.org/10.1007/s10853-006-0637-z>.
- [4] P. Duxson, J.L. Provis, G.C. Lukey, J.S.J. van Deventer, The role of inorganic polymer technology in the development of “green concrete,” *Cem. Concr. Res.* 37 (2007) 1590–1597. <https://doi.org/10.1016/j.cemconres.2007.08.018>.
- [5] S.A. Bernal, J.L. Provis, Durability of alkali-activated materials: Progress and perspectives, *J. Am. Ceram. Soc.* 97 (2014) 997–1008. <https://doi.org/10.1111/jace.12831>.

- [6] K. Arbi, M. Nedeljkovi, Y. Zuo, G. Ye, A review on the durability of alkali-activated fly ash/slag systems: Advances, issues, and perspectives, *Ind. Eng. Chem. Res.* 55 (2016) 5439–5453. <https://doi.org/10.1021/acs.iecr.6b00559>.
- [7] T. Gonçalves, R.V. Silva, J. de Brito, J.M. Fernández, A.R. Esquinas, Mechanical and durability performance of mortars with fine recycled concrete aggregates and reactive magnesium oxide as partial cement replacement, *Cem. Concr. Compos.* 105 (2020) 103420. <https://doi.org/10.1016/j.cemconcomp.2019.103420>.
- [8] S. A. Walling, H. Kinoshita, S. A. Bernal, N. C. Collier, J. L. Provis, Structure and properties of binder gels formed in the system $\text{Mg}(\text{OH})_2\text{-SiO}_2\text{-H}_2\text{O}$ for immobilisation of Magnox sludge, *Dalton Trans.* 44 (2015) 8126–8137. <https://doi.org/10.1039/C5DT00877H>.
- [9] S.A. Walling, J.L. Provis, Magnesia-Based Cements: A journey of 150 years, and cements for the future?, *Chem. Rev.* 116 (2016) 4170–4204. <https://doi.org/10.1021/acs.chemrev.5b00463>.
- [10] E. Bernard, B. Lothenbach, D. Rentsch, I. Pochard, A. Dauzères, Formation of magnesium silicate hydrates (M-S-H), *Phys. Chem. Earth Parts ABC.* 99 (2017) 142–157. <https://doi.org/10.1016/j.pce.2017.02.005>.
- [11] J. Szczerba, R. Prorok, E. Śnieżek, D. Madej, K. Maślona, Influence of time and temperature on ageing and phases synthesis in the $\text{MgO-SiO}_2\text{-H}_2\text{O}$ system, *Thermochim. Acta.* 567 (2013) 57–64.
- [12] D.R.M. Brew, F.P. Glasser, Synthesis and characterisation of magnesium silicate hydrate gels, *Cem. Concr. Res.* 35 (2005) 85–98. <https://doi.org/10.1016/j.cemconres.2004.06.022>.
- [13] E. Bernard, B. Lothenbach, C. Cau-Dit-Coumes, I. Pochard, D. Rentsch, Aluminum incorporation into magnesium silicate hydrate (M-S-H), *Cem. Concr. Res.* 128 (2020) 105931. <https://doi.org/10.1016/j.cemconres.2019.105931>.
- [14] A. Pedone, F. Palazzetti, V. Barone, Models of aged magnesium–silicate–hydrate cements based on the lizardite and talc crystals: A periodic DFT-GIPAW investigation, *J. Phys. Chem. C.* 121 (2017) 7319–7330. <https://doi.org/10.1021/acs.jpcc.7b00708>.
- [15] B. Lothenbach, D. Nied, E. L'Hôpital, G. Achiedo, A. Dauzères, Magnesium and calcium silicate hydrates, *Cem. Concr. Res.* 77 (2015) 60–68. <https://doi.org/10.1016/j.cemconres.2015.06.007>.
- [16] I.G. Richardson, A.R. Brough, R. Brydson, G.W. Groves, C.M. Dobson, Location of aluminum in substituted calcium silicate hydrate (C-S-H) gels as determined by ^{29}Si and ^{27}Al NMR and EELS, *J. Am. Ceram. Soc.* 76 (1993) 2285–2288. <https://doi.org/10.1111/j.1151-2916.1993.tb07765.x>.
- [17] S.D. Wang, K.L. Scrivener, ^{29}Si and ^{27}Al NMR study of alkali-activated slag, *Cem. Concr. Res.* 33 (2003) 769–774. [https://doi.org/10.1016/S0008-8846\(02\)01044-X](https://doi.org/10.1016/S0008-8846(02)01044-X).
- [18] X. Ke, M. Criado, J.L. Provis, S.A. Bernal, Slag-based cements that resist damage induced by carbon dioxide, *ACS Sustain. Chem. Eng.* 6 (2018) 5067–5075. <https://doi.org/10.1021/acssuschemeng.7b04730>.
- [19] M. Vespa, C. Borca, T. Huthwelker, B. Lothenbach, R. Dähn, E. Wieland, Structural characterisation of Magnesium (Sodium) Aluminium Silicate Hydrate (M-(N)-A-S-H) phases by X-ray absorption near-edge spectroscopy, *Appl. Geochem.* (2020) 104750. <https://doi.org/10.1016/j.apgeochem.2020.104750>.
- [20] M.B. Haha, B. Lothenbach, G. Le Saout, F. Winnefeld, Influence of slag chemistry on the hydration of alkali-activated blast-furnace slag - Part II: Effect of Al_2O_3 , *Cem. Concr. Res.* 42 (2012) 74–83. <https://doi.org/10.1016/j.cemconres.2011.08.005>.
- [21] S.A. Bernal, R. San Nicolas, R.J. Myers, R. Mejía De Gutiérrez, F. Puertas, J.S.J. Van Deventer, J.L. Provis, MgO content of slag controls phase evolution and structural changes induced by accelerated carbonation in alkali-activated binders, *Cem. Concr. Res.* 57 (2014) 33–43. <https://doi.org/10.1016/j.cemconres.2013.12.003>.
- [22] F. Winnefeld, M. Ben Haha, G. Le Saout, M. Costoya, S.C. Ko, B. Lothenbach, Influence of slag composition on the hydration of alkali-activated slags, *J. Sustain. Cem.-Based Mater.* 4 (2015) 85–100. <https://doi.org/10.1080/21650373.2014.955550>.
- [23] E. Bernard, B. Lothenbach, C. Cau-Dit-Coumes, C. Chlique, A. Dauzères, I. Pochard, Magnesium and calcium silicate hydrates, Part I: Investigation of the possible magnesium incorporation in

- calcium silicate hydrate (C-S-H) and of the calcium in magnesium silicate hydrate (M-S-H), *Appl. Geochem.* 89 (2018) 229–242. <https://doi.org/10.1016/j.apgeochem.2017.12.005>.
- [24] E. G. Ferreira, J. T. Marumo, M. K. Franco, F. Yokaichiya, and R. Vicente, “10000 years cement—Can hydrated cement last as much as long-lived radionuclides?,” *Cem. Concr. Compos.*, 103 (2019) 339–352.
- [25] H.A. Abdel-Gawwad, H.S. Hassan, S.R. Vásquez-García, I. Israde-Alcántara, Y.C. Ding, M.A. Martínez-Cinco, S. Abd El-Aleem, H.M. Khater, T.A. Tawfik, I.M. El-Kattan, Towards a clean environment: The potential application of eco-friendly magnesia-silicate cement in CO₂ sequestration, *J. Clean. Prod.* 252 (2020) 119875. <https://doi.org/10.1016/j.jclepro.2019.119875>.
- [26] M.P. Pechini, Method of preparing lead and alkaline earth titanates and niobates and coating method using the same to form a capacitor, US Patent #3330697 (1967).
- [27] J. Lin, M. Yu, C. Lin, X. Liu, Multifunctional oxide optical materials via the versatile pechini-type sol-gel process: Synthesis and characteristics, *J. Phys. Chem. C.* 111 (2007) 5835–5845. <https://doi.org/10.1021/jp070062c>.
- [28] S. Kumar Saha, A. Pathak, P. Pramanik, Low-temperature preparation of fine particles of mixed oxide systems, *J. Mater. Sci. Lett.* 14 (1995) 35–37. <https://doi.org/10.1007/BF02565279>.
- [29] P. Pramanik, A. Pathak, A new chemical route for the preparation of fine ferrite powders, *Bull. Mater. Sci.* 17 (1994) 967–975. <https://doi.org/10.1007/BF02757573>.
- [30] M. A. Gülgün, M.H. Nguyen, W.M. Kriven, Polymerized organic-inorganic synthesis of mixed oxides, *J. Am. Ceram. Soc.* 82 (1999) 556–560. <https://doi.org/10.1111/j.1151-2916.1999.tb01800.x>.
- [31] M.H. Nguyen, S.J. Lee, W.M. Kriven, Synthesis of oxide powders by way of a polymeric steric entrapment precursor route, *J. Mater. Res.* 14 (1999) 3417–3426. <https://doi.org/10.1557/JMR.1999.0462>.
- [32] S.J. Lee, W.M. Kriven, Crystallization and densification of nano-size amorphous cordierite powder prepared by a PVA solution-polymerization route, *J. Am. Ceram. Soc.* (2005). <https://doi.org/10.1111/j.1151-2916.1998.tb02667.x>.
- [33] B. Walkley, R. San Nicolas, M.A. Sani, J.D. Gehman, J.S.J. van Deventer, J.L. Provis, Synthesis of stoichiometrically controlled reactive aluminosilicate and calcium-aluminosilicate powders, *Powder Technol.* 297 (2016) 17–33. <https://doi.org/10.1016/j.powtec.2016.04.006>.
- [34] B. Walkley, R. San Nicolas, M.A. Sani, S.A. Bernal, J.S.J. van Deventer, J.L. Provis, Structural evolution of synthetic alkali-activated CaO-MgO-Na₂O-Al₂O₃-SiO₂ materials is influenced by Mg content, *Cem. Concr. Res.* 99 (2017) 155–171. <https://doi.org/10.1016/j.cemconres.2017.05.006>.
- [35] B. Walkley, R. San Nicolas, M.A. Sani, J.D. Gehman, J.S.J. Van Deventer, J.L. Provis, Phase evolution of Na₂O-Al₂O₃-SiO₂-H₂O gels in synthetic aluminosilicate binders, *Dalton Trans.* 45 (2016) 5521–5535. <https://doi.org/10.1039/c5dt04878h>.
- [36] S.J. Lee, E. A. Benson, W.M. Kriven, Preparation of portland cement components by poly(vinyl alcohol) solution polymerization, *J. Am. Ceram. Soc.* 82 (1999) 2049–2055. <https://doi.org/10.1111/j.1151-2916.1999.tb02039.x>.
- [37] J.P. Gevaudan, J.D. Wallat, B. Lama, W.V. Srubar, PVA- and PEG-assisted sol-gel synthesis of aluminosilicate precursors for N-A-S-H geopolymer cements, *J. Am. Ceram. Soc.* 103 (2020) 859–877. <https://doi.org/10.1111/jace.16764>.
- [38] J.P. Gevaudan, K.M. Campbell, T.J. Kane, R.K. Shoemaker, W. V. Srubar, Mineralization dynamics of metakaolin-based alkali-activated cements, *Cem. Concr. Res.* 94 (2017) 1–12. <https://doi.org/10.1016/j.cemconres.2017.01.001>.
- [39] J. Osio-Norgaard, J.P. Gevaudan, W.V. Srubar, A review of chloride transport in alkali-activated cement paste, mortar, and concrete, *Constr. Build. Mater.* 186 (2018) 191–206. <https://doi.org/10.1016/j.conbuildmat.2018.07.119>.
- [40] F. Jin, K. Gu, A. Al-Tabbaa, Strength and drying shrinkage of reactive MgO modified alkali-activated slag paste, *Constr. Build. Mater.* 51 (2014) 395–404. <https://doi.org/10.1016/j.conbuildmat.2013.10.081>.

- [41] J. Brus, S. Abbrent, L. Kobera, M. Urbanova, Advances in ^{27}Al MAS NMR studies of geopolymers, *Ann. Rep. NMR Spect.* 88 (2016) 79-147.
- [42] D.E. Woessner, Characterization of clay minerals by ^{27}Al nuclear magnetic resonance spectroscopy, *Am. Mineral.* 74 (1989) 203–215.
- [43] B.T. Poe, P.F. McMillan, C.A. Angell, R.K. Sato, Al and Si coordination in $\text{SiO}_2\text{-Al}_2\text{O}_3$ glasses and liquids: A study by NMR and IR spectroscopy and MD simulations, *Chem. Geol.* 96 (1992) 333–349. [https://doi.org/10.1016/0009-2541\(92\)90063-B](https://doi.org/10.1016/0009-2541(92)90063-B).
- [44] P. Tarte, Infrared spectra of inorganic aluminates and characteristic vibrational frequencies of AlO_4 tetrahedra and AlO_6 octahedra, *Spect. Act Part A: Mol Spect.* 23 (1966) 2127–2143.
- [45] W.R. Taylor, Application of infrared spectroscopy to studies of silicate glass structure: Examples from the melilite glasses and the systems $\text{Na}_2\text{O-SiO}_2$ and $\text{Na}_2\text{O-Al}_2\text{O}_3\text{-SiO}_2$, *Proc Indian Acad Sci.* 99 (1990) 99–117. <https://doi.org/10.1007/BF00462802>.
- [46] R.J. Myers, S.A. Bernal, R. San Nicolas, J.L. Provis, Generalized structural description of calcium–sodium aluminosilicate hydrate gels: The cross-linked substituted tobermorite model, *Langmuir.* 29 (2013) 5294–5306. <https://doi.org/10.1021/la4000473>.
- [47] A. Fernández-Jiménez, F. Puertas, I. Sobrados, J. Sanz, Structure of calcium silicate hydrates formed in alkaline-activated slag: Influence of the type of alkaline activator, *J. Am. Ceram. Soc.* 86 (2003) 1389–1394. <https://doi.org/10.1111/j.1151-2916.2003.tb03481.x>.
- [48] B. Walkley, S.J. Page, G.J. Rees, J.L. Provis, J.V. Hanna, Nanostructure of $\text{CaO-(Na}_2\text{O)-Al}_2\text{O}_3\text{-SiO}_2\text{-H}_2\text{O}$ gels revealed by multinuclear solid-state magic angle spinning and multiple quantum magic angle spinning nuclear magnetic resonance spectroscopy, *J. Phys. Chem. C.* 124 (2020) 1681–1694. <https://doi.org/10.1021/acs.jpcc.9b10133>.
- [49] P. Duxson, G.C. Lukey, F. Separovic, J.S.J. Van Deventer, Effect of alkali cations on aluminum incorporation in geopolymeric gels, (2005) 832–839. <https://doi.org/10.1021/ie0494216>.
- [50] J. Klinowski, Nuclear Magnetic Resonance Studies of Zeolites, *Prog. NMR Spectrosc.* 16 (1984) 237–309.
- [51] J.D.K. MacKenzie, M.E. Smith, Multinuclear Solid-State NMR of Inorganic Materials, Pergamon Mater. Ser. 6 (2002) 201–268. [https://doi.org/10.1016/S1470-1804\(02\)80005-0](https://doi.org/10.1016/S1470-1804(02)80005-0).
- [52] E. Lippmaa, M. Magi, M. Tarmak, W. Wiekler, A.R. Grimmer, D.M. Roy, A high Resolution ^{29}Si NMR study of the hydration of tricalciumsilicate, *Cem. Concr. Res.* 12 (1982) 597–602.
- [53] A.M.B. Silva, C.M. Queiroz, S. Agathopoulos, R.N. Correia, M.H.V. Fernandes, J.M. Oliveira, Structure of $\text{SiO}_2\text{-MgO-Na}_2\text{O}$ glasses by FTIR, Raman and ^{29}Si MAS NMR, *J. Mol. Struct.* 986 (2011) 16–21. <https://doi.org/10.1016/j.molstruc.2010.11.023>.
- [54] H. Yang, R.I. Walton, S. Antonijevic, S. Wimperis, A.C. Hannon, Local order of amorphous zeolite precursors from $^{29}\text{Si}\{^1\text{H}\}$ CPMAS and ^{27}Al and ^{23}Na MQMAS NMR and evidence for the nature of medium-range order from neutron diffraction, *J. Phys. Chem. B.* 108 (2004) 8208–8217. <https://doi.org/10.1021/jp037887g>.
- [55] J.B. d’Espinoze de la Caillerie, M. Kermarec, O. Clause, ^{29}Si NMR observation of an amorphous magnesium silicate formed during impregnation of silica with Mg(II) in aqueous solution, *J. Phys. Chem.* 99 (1995) 17273–17281. <https://doi.org/10.1021/j100047a036>.
- [56] E. Pustovgar, R.P. Sangodkar, A.S. Andreev, M. Palacios, B.F. Chmelka, R.J. Flatt, J.E. De Lacaillerie, Understanding silicate hydration from quantitative analyses of hydrating tricalcium silicates, *Nat. Commun.* (2016) 1–9. <https://doi.org/10.1038/ncomms10952>.
- [57] R. Oberti, L. Ungaretti, A. Tlili, D.C. Smith, J.L. Robert, The crystal structure of preiswerkite, *Am. Mineral.* 78 (1993) 1290–1298.
- [58] S.D. Wang, K.L. Scrivener, Hydration products of alkali activated slag cement, *Cem. Concr. Res.* 25 (1995) 561-567.
- [59] C. Roosz, S. Grangeon, P. Blanc, V. Montouillout, B. Lothenbach, P. Henocq, E. Giffaut, P. Vieillard, S. Gaboreau, Crystal structure of magnesium silicate hydrates (M-S-H): The relation

- with 2:1 Mg–Si phyllosilicates, *Cem. Concr. Res.* 73 (2015) 228–237. <https://doi.org/10.1016/j.cemconres.2015.03.014>.
- [60] C. Roosz, P. Vieillard, P. Blanc, S. Gaboreau, H. Gailhanou, D. Braithwaite, V. Montouillout, R. Denoyel, P. Henocq, B. Madé, Thermodynamic properties of C-S-H, C-A-S-H and M-S-H phases: Results from direct measurements and predictive modelling, *Appl. Geochem.* 92 (2018) 140–156. <https://doi.org/10.1016/j.apgeochem.2018.03.004>.
- [61] M.R. Rowles, J.V. Hanna, K.J. Pike, M.E. Smith, B.H. O'Connor, ^{29}Si , ^{27}Al , ^1H and ^{23}Na MAS NMR study of the bonding character in aluminosilicate inorganic polymers, *Appl. Magn. Reson.* 32 (2007) 663–689. <https://doi.org/10.1007/s00723-007-0043-y>.
- [62] C.E. Tambelli, J.F. Schneider, N.P. Hasparyk, P.J.M. Monteiro, Study of the structure of alkali–silica reaction gel by high-resolution NMR spectroscopy, *J. Non-Cryst. Solids.* 352 (2006) 3429–3436. <https://doi.org/10.1016/j.jnoncrysol.2006.03.112>.
- [63] X. Xue, J.F. Stebbins, ^{23}Na NMR chemical shifts and local Na coordination environments in silicate crystals, melts and glasses, *Phys. Chem. Miner.* 20 (1993) 297–307.
- [64] D. Nied, K. Enemark-Rasmussen, E. L'Hopital, J. Skibsted, B. Lothenbach, Properties of magnesium silicate hydrates (M-S-H), *Cem. Concr. Res.* 79 (2016) 323–332. <https://doi.org/10.1016/j.cemconres.2015.10.003>.
- [65] S.A. Bernal, J.L. Provis, V. Rose, R. Mejía De Gutierrez, Evolution of binder structure in sodium silicate-activated slag-metakaolin blends, *Cem. Concr. Compos.* 33 (2011) 46–54. <https://doi.org/10.1016/j.cemconcomp.2010.09.004>.
- [66] I. García Lodeiro, A. Fernández-Jimenez, A. Palomo, D.E. Macphee, Effect on fresh C-S-H gels of the simultaneous addition of alkali and aluminium, *Cem. Concr. Res.* 40 (2010) 27–32. <https://doi.org/10.1016/j.cemconres.2009.08.004>.
- [67] W.K.W. Lee, J.S.J. Van Deventer, Use of infrared spectroscopy to study geopolymerization of heterogeneous amorphous aluminosilicates, *Langmuir.* 19 (2003) 8726–8734. <https://doi.org/10.1021/la026127e>.
- [68] R. Hanna, G. J. Su, Infrared absorption spectra of sodium silicate glasses from 4 to 30 μm , *J. Am. Ceram. Soc.* 47 (1964) 597–601. <https://doi.org/10.1111/j.1151-2916.1964.tb13113.x>.
- [69] R.K. Vempati, A. Rao, T.R. Hess, D.L. Cofke, Fraction and characterization of Texas lignite class 'F' fly ash by XRD, TGA, FTIR and SFM, *Cem. Concr. Res.* 24 (1994) 1153–1164.
- [70] M.Y.A. Mollah, T.R. Hess, D.L. Cofke, Surface and bulk studies of leached and unleached fly ash using XPS, SEM, EDS, and FTIR techniques, *Cem. Concr. Res.* 24 (1994) 109–118.
- [71] T. Uchino, T. Sakka, M. Iwasaki, Interpretation of hydrated states of sodium silicate glasses by infrared and raman analysis, *J. Am. Ceram. Soc.* 74 (1991) 306–313. <https://doi.org/10.1111/j.1151-2916.1991.tb06880.x>.
- [72] I. García-Lodeiro, A. Fernández-Jiménez, M.T. Blanco, A. Palomo, FTIR study of the sol-gel synthesis of cementitious gels: C-S-H and N-A-S-H, *J. Sol-Gel Sci. Technol.* 45 (2008) 63–72. <https://doi.org/10.1007/s10971-007-1643-6>.
- [73] I. Giannopoulou, D. Papanias, Hydrolytic stability of sodium silicate gels in the presence of aluminum, *J. Mater. Sci.* 45 (2010) 5370–5377. <https://doi.org/10.1007/s10853-010-4586-1>.
- [74] F.M. Ernsberger, Molecular Water in Glass, *J. Am. Ceram. Soc.* 60 (1977) 91–92. <https://doi.org/10.1111/j.1151-2916.1977.tb16110.x>.
- [75] P. Yu, R.J. Kirkpatrick, B. Poe, P.F. McMillan, X. Cong, Structure of calcium silicate hydrate (C-S-H): Near-, mid-, and far-infrared spectroscopy, *J. Am. Ceram. Soc.* 82 (1999) 742–748. <https://doi.org/10.1111/j.1151-2916.1999.tb01826.x>.
- [76] V.A. Walters, D.L. Snavely, S.D. Colson, K.B. Wiberg, K.N. Wong, New vibrational constants for pyridine from low-temperature and high-resolution infrared spectra, *J. Phys. Chem.* 90 (1986) 592–597. <https://doi.org/10.1021/j100276a022>.
- [77] B. Focher, A. Naggi, G. Torri, A. Cosani, M. Terbojevich, Structural differences between chitin polymorphs and their precipitates from solutions-evidence from CP-MAS ^{13}C -NMR, FT-IR and

- FT-Raman spectroscopy, *Carbohydr. Polym.* 17 (1992) 97–102. [https://doi.org/10.1016/0144-8617\(92\)90101-U](https://doi.org/10.1016/0144-8617(92)90101-U).
- [78] K.M. Atkins, R.N. Edmonds, A.J. Majumdar, The hydration of Portland and aluminous cements with added polymer dispersions, *J. Mater. Sci.* 26 (1991) 2372–2378. <https://doi.org/10.1007/BF01130184>.
- [79] C. Chen, C. Ho, C.D. Chen, Physicochemical properties of calcium silicate cements for endodontic treatment, *J. Endod.* 35 (2009) 1288–1291. <https://doi.org/10.1016/j.joen.2009.05.036>.
- [80] A.R. Davis, B.G. Oliver, A vibrational-spectroscopic study of the species present in the CO₂-H₂O system, *J. Solut. Chem.* 1 (1972) 329–339. <https://doi.org/10.1007/bf00715991>.
- [81] J. Laane, J.R. Ohlsen, Characterization of nitrogen oxides by vibrational spectroscopy, *Prog. Inorg. Chem.* 27 (1980) 465–513.
- [82] M. Zhang, Q. Hui, X.J. Lou, S.A.T. Redfern, E.K.H. Salje, S.C. Tarantino, Dehydroxylation, proton migration, and structural changes in heated talc: An infrared spectroscopic study, *Am. Mineral.* 91 (2006) 816–825. <https://doi.org/10.2138/am.2006.1945>.
- [83] B. Lafuente, R.T. Downs, H. Yang, N. Stone, The power of databases: The RRUFF project, in: T. Armbruster, R.M. Danisi (Eds.), *Highlights Mineral. Crystallogr.*, De Gruyter, Berlin, Germany, 2015: pp. 1–30. <https://doi.org/10.1515/9783110417104-003>.
- [84] J.R. Ferraro, M.H. Manghnani, Infrared absorption spectra of sodium silicate glasses at high pressures, *J. Appl. Phys.* 43 (1972) 4595–4599. <https://doi.org/10.1063/1.1660971>.
- [85] R.M. Almeida, T.A. Guiton, C.G. Pantano, Characterization of silica gels by infrared reflection spectroscopy, *J. Non-Cryst. Solids.* 121 (1990) 193–197. [https://doi.org/10.1016/0022-3093\(90\)90130-E](https://doi.org/10.1016/0022-3093(90)90130-E).
- [86] A.M.B. Silva, M.H.V. Fernandes, J.M. Oliveira, C.M. Queiroz, R.N. Correia, S. Agathopoulos, Structure of SiO₂-MgO-Na₂O glasses by FTIR, Raman and ²⁹Si MAS NMR, *J. Mol. Struct.* 986 (2010) 16–21. <https://doi.org/10.1016/j.molstruc.2010.11.023>.
- [87] M.E. Simonsen, C. Sønderby, Z. Li, E.G. Søgaard, XPS and FT-IR investigation of silicate polymers, *J. Mater. Sci.* 44 (2009) 2079–2088. <https://doi.org/10.1007/s10853-009-3270-9>.
- [88] T. Uchino, T. Sakka, K. Hotta, Attenuated total reflectance fourier-transform infrared spectra of a hydrated sodium silicate glass, *J. Am. Cer. Soc.* 72 (1989) 2713–2715.
- [89] J.M. Saniger, Al-O infrared vibrational frequencies of γ -alumina, *Mater. Lett.* 22 (1995) 109–113. [https://doi.org/10.1016/0167-577X\(94\)00234-7](https://doi.org/10.1016/0167-577X(94)00234-7).
- [90] J. Buhl, The properties of salt-filled sodalites. Part 3. Synthesis and thermal behaviour of basic and non-basic carbonate enclathrated sodalites, *Thermochm. Act.* 219 (1993) 205–214.
- [91] G. Bergeret, T.M. Tri, P. Gallezot, X-ray study of palladium location in Y zeolite during in situ hydrogen reduction, benzene adsorption, and benzene hydrogenation, *J. Phys. Chem.* (1983). <https://doi.org/10.1021/j100230a013>.
- [92] M. Criado, A. Fernández-Jiménez, A. Palomo, Alkali activation of fly ash: Effect of the SiO₂/Na₂O ratio, *Microporous Mesoporous Mater.* 106 (2007) 180–191. <https://doi.org/10.1016/j.micromeso.2007.02.055>.
- [93] M. Criado, A. Fernández-Jiménez, A.G. de la Torre, M.A.G. Aranda, A. Palomo, An XRD study of the effect of the SiO₂/Na₂O ratio on the alkali activation of fly ash, *Cem. Concr. Res.* 37 (2007) 671–679. <https://doi.org/10.1016/j.cemconres.2007.01.013>.
- [94] A. Fernández-Jiménez, A. Palomo, Composition and microstructure of alkali activated fly ash binder: Effect of the activator, *Cem. Concr. Res.* 35 (2005) 1984–1992. <https://doi.org/10.1016/j.cemconres.2005.03.003>.
- [95] B. Walkley, G.J. Rees, R. San Nicolas, J.S.J. van Deventer, J.V. Hanna, J.L. Provis, New structural model of hydrous sodium aluminosilicate gels and the role of charge-balancing extra-framework Al, *J. Phys. Chem. C.* 122 (2018) 5673–5685. <https://doi.org/10.1021/acs.jpcc.8b00259>.
- [96] Z. Yang, H. Fischer, R. Polder, Synthesis and characterization of modified hydrotalcites and their ion exchange characteristics in chloride-rich simulated concrete pore solution, *Cem. Concr. Compos.* 47 (2014) 87–93. <https://doi.org/10.1016/j.cemconcomp.2013.03.008>.

- [97] J.G. Thompson, A. Melnitchenko, S.R. Palethorpe, R.L. Withers, An XRD and electron diffraction study of cristobalite-related phases in the $\text{NaAlO}_2\text{-NaAlSiO}_4$ system, *J. Solid State Chem.* 131 (1997) 24–37. <https://doi.org/10.1006/jssc.1997.7295>.
- [98] J.H. Carman, Synthetic sodium phlogopite and its two hydrates: Stabilities, properties, and mineralogic implications, *Am. Mineral.* 59 (1974) 261–273.
- [99] K.J. MacKenzie, S. Bradley, J.V. Hanna, M.E. Smith, Magnesium analogues of aluminosilicate inorganic polymers (geopolymers) from magnesium minerals, *J. Mater. Sci.* 48 (2013) 1787–1793.
- [100] J. Temuujin, K. Okada, K.J.D. MacKenzie, Formation of layered magnesium silicate during the aging of magnesium hydroxide-silica mixtures, *J. Am. Ceram. Soc.* 81 (2005) 754–756. <https://doi.org/10.1111/j.1151-2916.1998.tb02405.x>.
- [101] M. Tonelli, F. Martini, L. Calucci, E. Fratini, M. Geppi, F. Ridi, S. Borsacchi, P. Baglioni, Structural characterization of magnesium silicate hydrate: towards the design of eco-sustainable cements, *Dalton Trans.* 45 (2016) 3294–3304. <https://doi.org/10.1039/C5DT03545G>.
- [102] P. Duxson, G.C. Lukey, J.S.J. van Deventer, Thermal evolution of metakaolin geopolymers: Part 1 - Physical evolution, *J. Non-Cryst. Solids.* 352 (2006) 5541–5555. <https://doi.org/10.1016/j.jnoncrysol.2006.09.019>.
- [103] J.L. Provis, R.M. Harrex, S.A. Bernal, P. Duxson, J.S.J. Van Deventer, Dilatometry of geopolymers as a means of selecting desirable fly ash sources, *J. Non-Cryst. Solids.* 358 (2012) 1930–1937. <https://doi.org/10.1016/j.jnoncrysol.2012.06.001>.
- [104] E.D. Rodríguez, S.A. Bernal, J.L. Provis, J. Paya, J.M. Monzo, M.V. Borrachero, Effect of nanosilica-based activators on the performance of an alkali-activated fly ash binder, *Cem. Concr. Compos.* 35 (2013) 1–11. <https://doi.org/10.1016/j.cemconcomp.2012.08.025>.
- [105] A.D. Chandwankar, S.B. Kulkari, Thermal behavior of modified faujasites, *J. Therm. Anal.* 19 (1980) 313–320.
- [106] I. V. Mishin, G.A. Piloyan, A.L. Klyachko, A.M. Rubinshtein, Study of decationized and dealuminized mordenites by the differential-thermal analysis method and measurement of water vapor absorption, *Bull. Acad. Sci. USSR, div. chem. sci.* 22 (1973) 1343–1345.
- [107] S.E. Wallah, D. Hardjito, Assessing the shrinkage and creep of alkali-activated concrete binders, Woodhead Publishing Limited, 2014. <https://doi.org/10.1533/9781782422884.2.265>.
- [108] R.I. Gilbert, Creep and shrinkage models for high strength concrete – Proposals for inclusion in AS3600, *Aust. J. Struct. Eng.* 4 (2017) 95–106. <https://doi.org/10.1080/13287982.2002.11464911>.
- [109] P. Duxson, G.C. Lukey, J.S.J. Van Deventer, Nanostructural design of multifunctional geopolymeric materials, *Ceram. Trans.* 175 (2006) 203–214.